

Supplementary Information

Bi-doped Ruthenium Oxide Nanocrystal for Water Oxidation in Acidic Media

Shiyao Chen^a, Hai Liu^a, Bichen Yuan^a, Wenhui Xu^a, Aiqing Cao^a, Marshet Getaye Sendeku^b,
Yaping Li^{a,*}, Xiaoming Sun^{a,*}, Fengmei Wang^{a,*}

a. State Key Laboratory of Chemical Resource Engineering, College of Chemistry, Beijing University of Chemical Technology, Beijing 100029, P. R. China.

b. Ocean Hydrogen Energy R&D Center, Research Institute of Tsinghua University in Shenzhen, Shenzhen, P. R. China.

*E-mail: wangfm@buct.edu.cn; sunxm@mail.buct.edu.cn; liyp@mail.buct.edu.cn

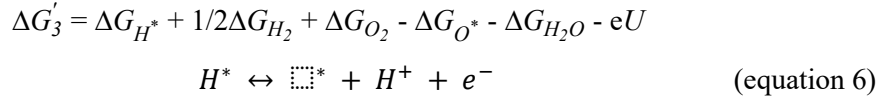
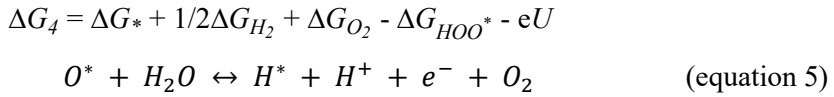
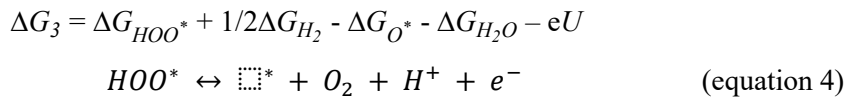
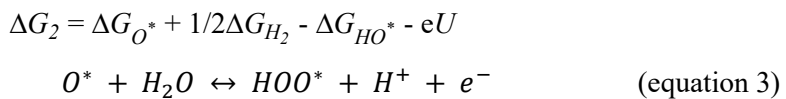
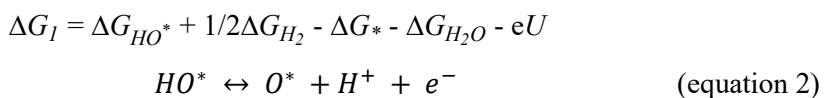
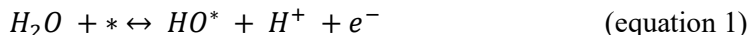
Supplementary Note 1

The Gibbs free energy of absorbed species (G_{*ads}) can be computed using following equation¹:

$$G_{*ads} = E + ZPE - TS$$

In this equation, $*ads$ represents the adsorbed species, such as $*OH$, $*O$, $*OOH$, or $*H$. The term G represents the Gibbs free energy of the adsorbed species, while E refers to the energy obtained from Density Functional Theory (DFT) calculation, ZPE stands for zero-point energy, S represents entropy and T denotes the temperature, which was set at 298.15 K for this study.

The oxygen evolution reaction (OER) under acidic conditions, a four-electron transfer process, comprises four distinct reaction steps (Figure 4a, 4b). Both AEM and LOM mechanisms share the common initial stages, which are evaluated using Equations 1 and 2. Subsequently, AEM proceeds with the next two stages, calculated by Equations 3 and 4 (Figure 4a),² whereas LOM continues with Equations 5 and 6 (Figure 4b).³ The Gibbs free energy of $(H^+ + e^-)$ at standard conditions is assumed as the free energy of $1/2 H_2$.



In this work, $\Delta G_{I-4}^{(j)}$ values were calculated at $U=0$ V.

Supplementary Note 2

To clarify the effect of varying loadings on the activity of the $\text{Bi}_{0.05}\text{Ru}_{0.95}\text{O}_2$ catalyst, the Turnover Frequency (TOF) value was calculated.

$$\text{TOF} = \frac{J*A}{4*e*n}$$

J is current density obtained at 1.5 V (vs. RHE) and normalized by geometric area; A is the geometric area; e is the charge of electron ($1.602 * 10^{-19}$ C) and n is the number of active sites, calculated *via* the following equation.

This method is calculating based on all Ru atoms, from the following equation:

$$n = \frac{m_{loading} * N_A}{M_w} * n_{metal}$$

where $m_{loading}$ is the loading mass of catalyst on carbon paper, n_{metal} is the mole number of metal atoms such as Ru per mole of electrocatalysts and M_w is the molecular weight of catalyst.

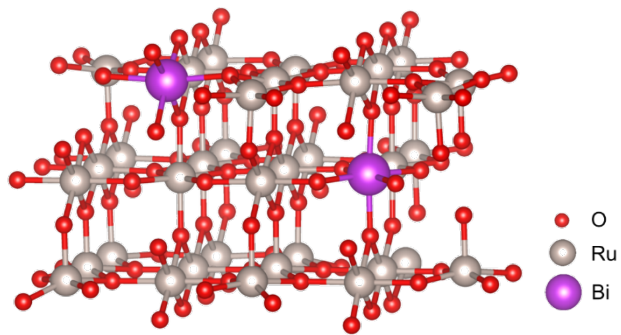


Figure S1 Slab model of $\text{Bi}_2\text{Ru}_{34}\text{O}_{72}$ after structural optimization.

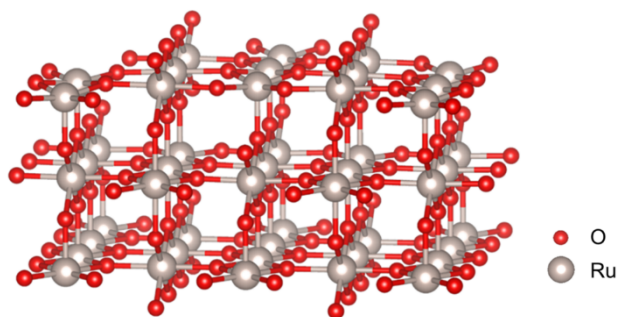


Figure S2 Slab model of RuO_2 after structural optimization.

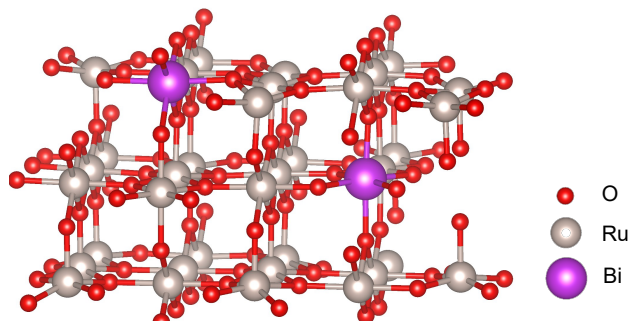


Figure S3 Slab model of $\text{Bi}-\text{O}_v-\text{RuO}_2$ after structural optimization.

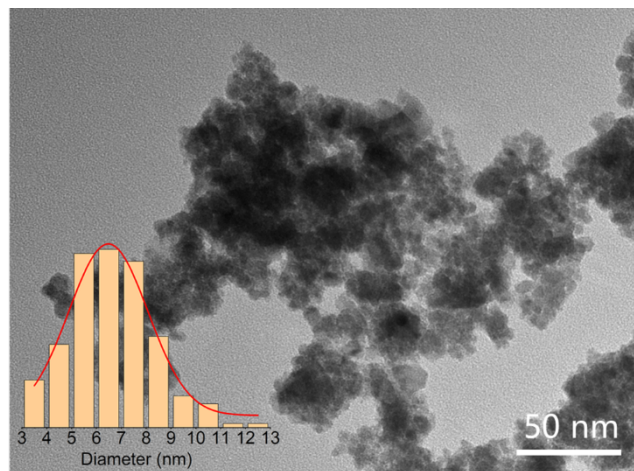


Figure S4 TEM image of $\text{Bi}_{0.05}\text{Ru}_{0.95}\text{O}_2$, inset showing particle size distribution.

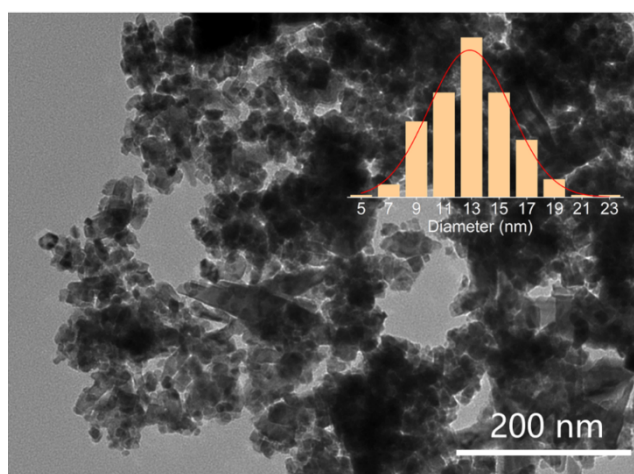


Figure S5 TEM image of HM- RuO_2 , inset showing particle size distribution.

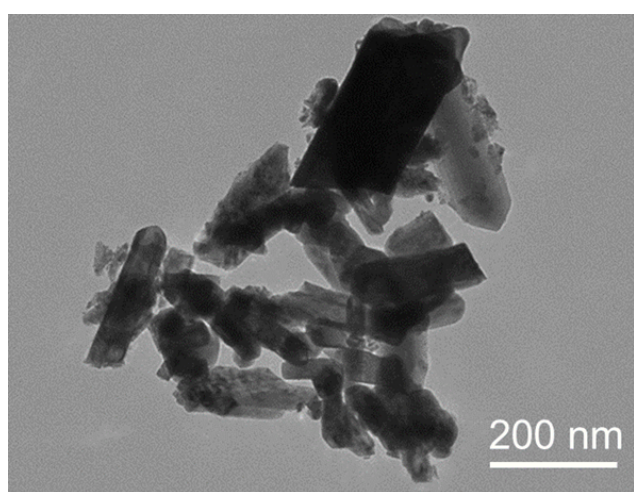


Figure S6 TEM image of C- RuO_2 .

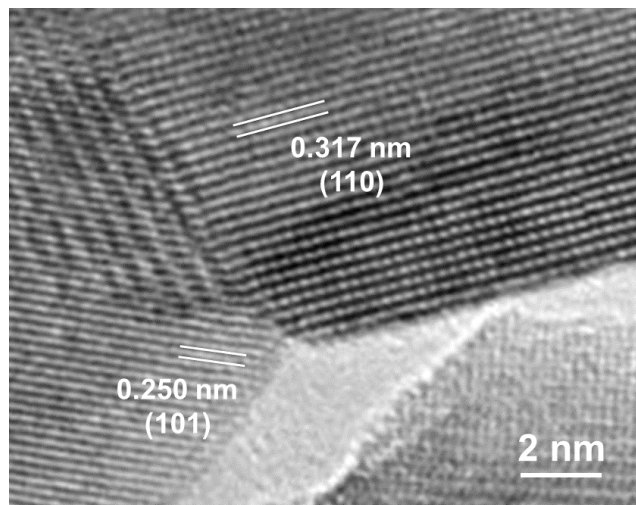


Figure S7 HRTEM image of C-RuO₂.

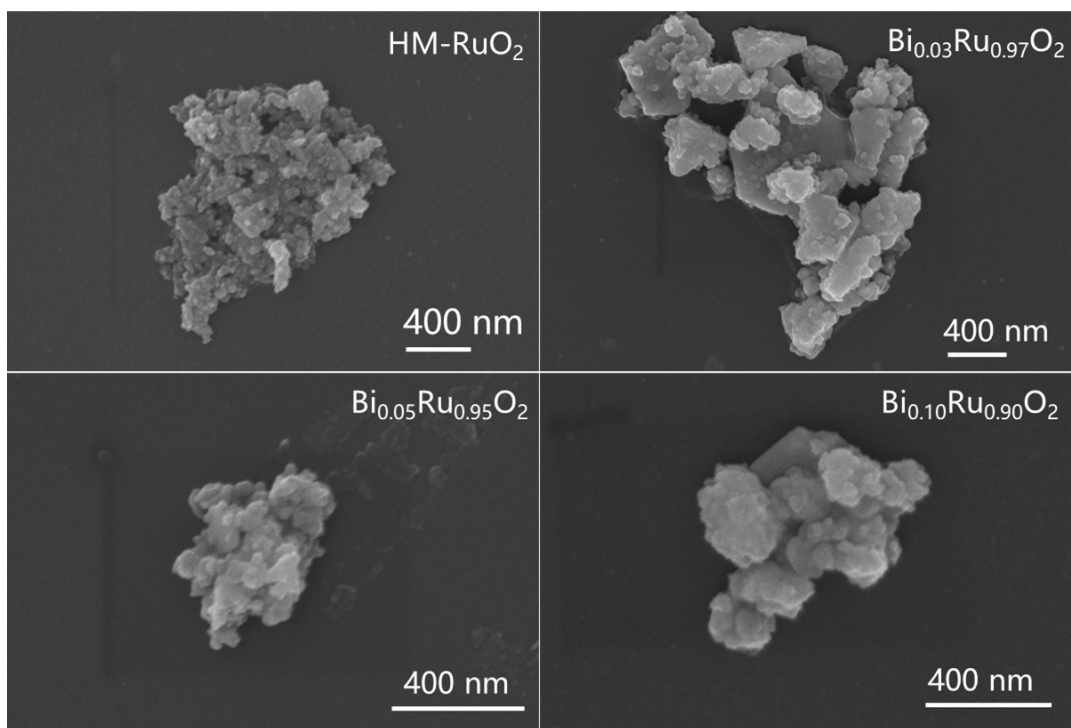


Figure S8 SEM images of HM-RuO₂, Bi_{0.03}Ru_{0.97}O₂, Bi_{0.05}Ru_{0.95}O₂, Bi_{0.10}Ru_{0.90}O₂.

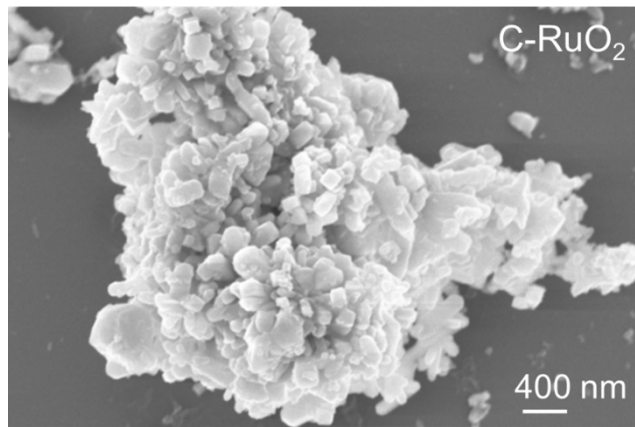


Figure S9 SEM image of C-RuO₂.

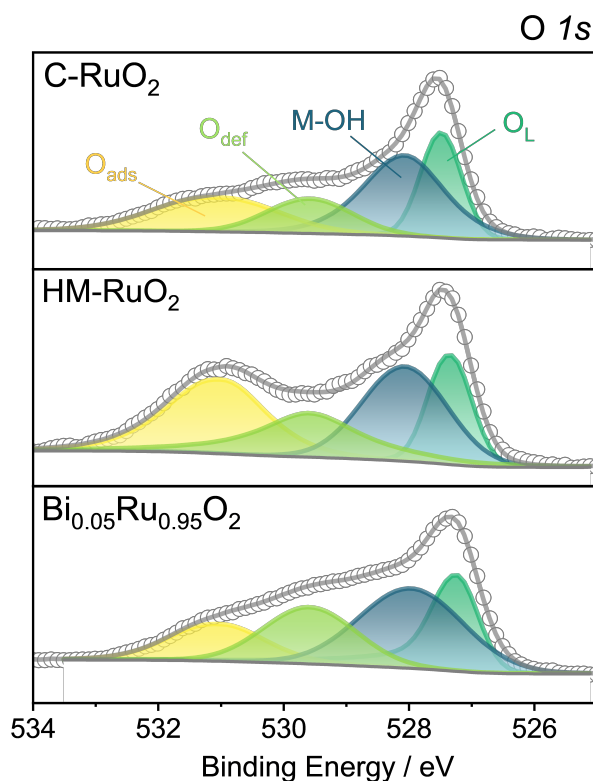


Figure S10 O 1s XPS spectra of $\text{Bi}_{0.05}\text{Ru}_{0.95}\text{O}_2$, HM-RuO₂ and C-RuO₂. More details are shown in Table S2.

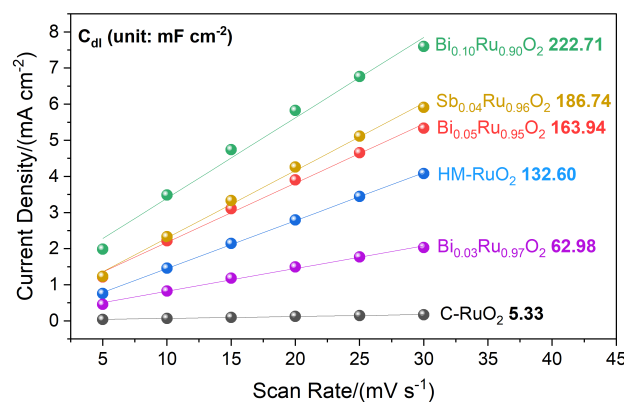


Figure S11 C_{dl} linear fitting plot of $\text{Bi}_x\text{Ru}_{1-x}\text{O}_2$, $\text{Sb}_{0.04}\text{Ru}_{0.96}\text{O}_2$, HM-RuO₂ and C-RuO₂ derived from CV curves.

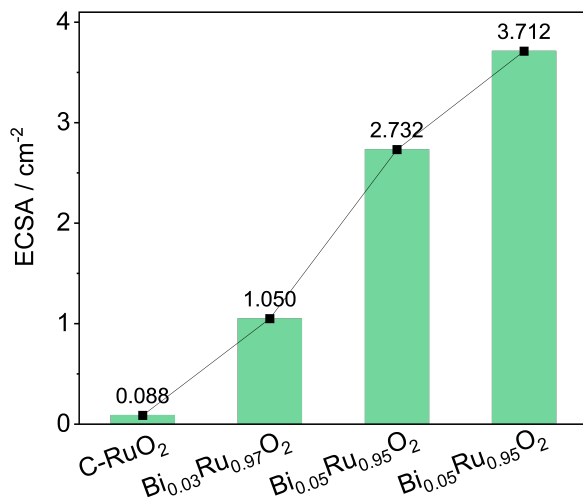


Figure S12 Comparison of electrochemical active surface areas of $\text{Bi}_x\text{Ru}_{1-x}\text{O}_2$ and C-RuO₂.

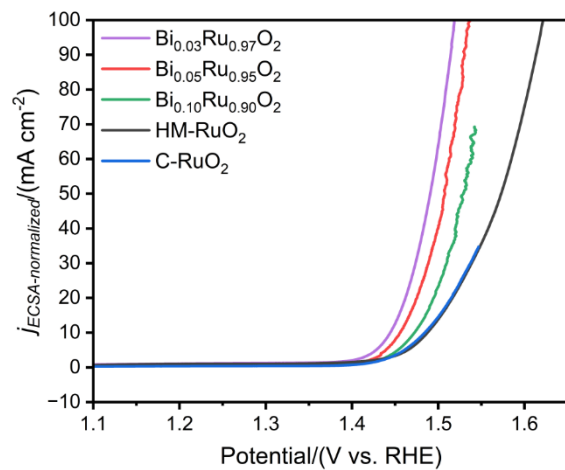


Figure S13 Specific activity curves of $\text{Bi}_x\text{Ru}_{1-x}\text{O}_2$, HM-RuO₂ and C-RuO₂ electrode collected at the scan rate of 5 mV s⁻¹ in 0.5 M H₂SO₄ electrolyte.

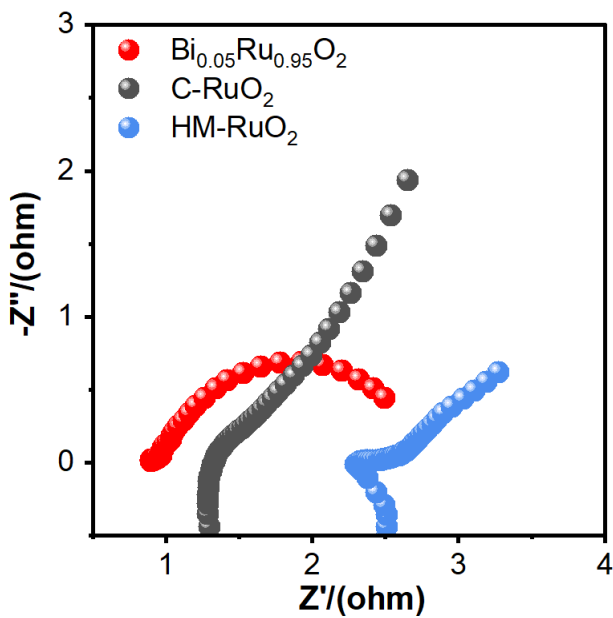


Figure S14 EIS plot of $\text{Bi}_{0.05}\text{Ru}_{0.95}\text{O}_2$, HM-RuO₂ and C-RuO₂ at a voltage (init E) of 1.24 V in 0.5 M H₂SO₄ electrolyte. The frequency range for testing is from 100 kHz to 1 Hz.

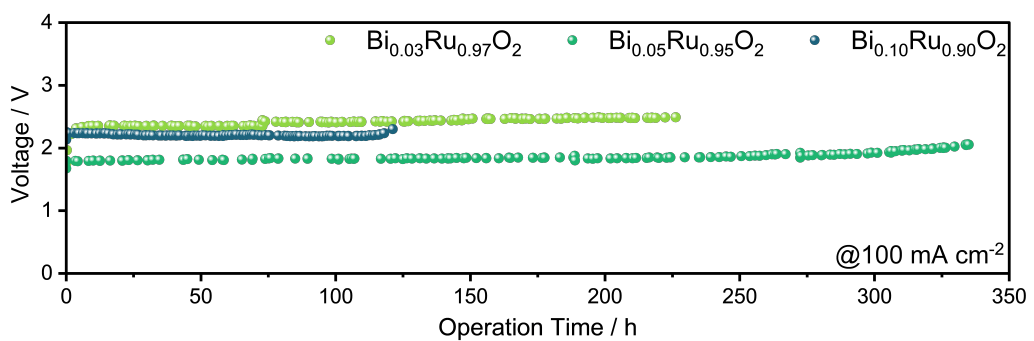


Figure S15 Chronopotentiometry tests of $\text{Bi}_x\text{Ru}_{1-x}\text{O}_2$ at 100 mA cm^{-2} in $0.5 \text{ M H}_2\text{SO}_4$ electrolyte.

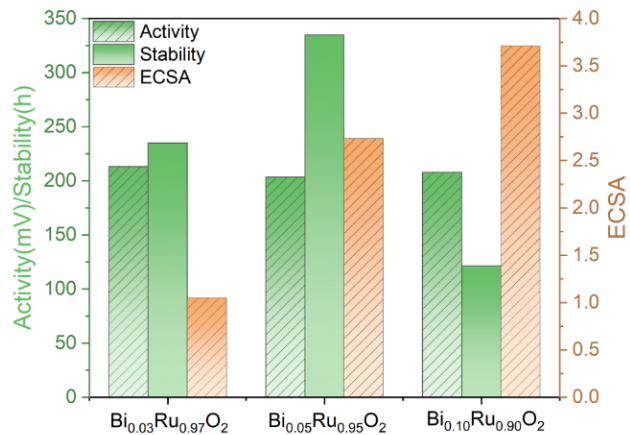


Figure S16 Comparison of activity (overpotential@10 mA cm⁻²) and stability (at 100 mA cm⁻²) among various $\text{Bi}_x\text{Ru}_{1-x}\text{O}_2$.

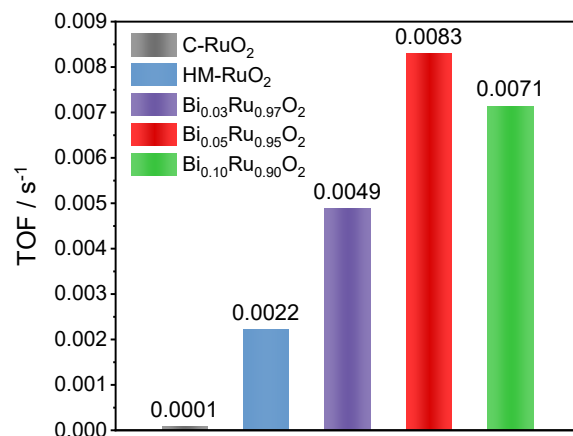


Figure S17 Turnover frequency comparison of $\text{Bi}_x\text{Ru}_{1-x}\text{O}_2$, HM-RuO₂ and C-RuO₂.

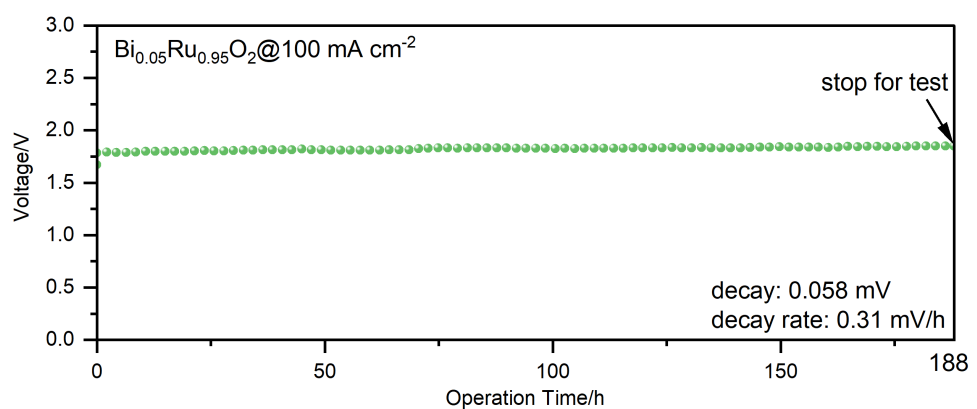


Figure S18 Chronopotentiometry test of $\text{Bi}_{0.05}\text{Ru}_{0.95}\text{O}_2$ in 0.5 M H_2SO_4 electrolyte at 100 mA cm^{-2} for 188 h. The electrode after the stability test was used for subsequent tests.

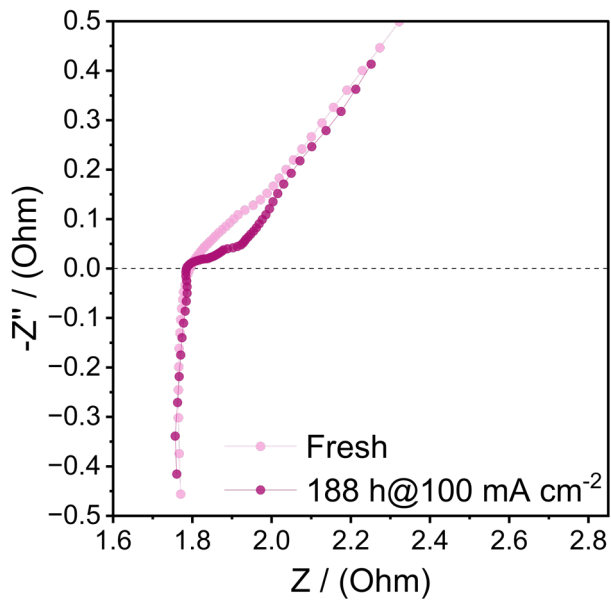


Figure S19 EIS plots of $\text{Bi}_{0.05}\text{Ru}_{0.95}\text{O}_2$ at a voltage (init E) of 1.24 V in 0.5 M H_2SO_4 electrolyte before and after 188-h stability test at 100mA cm^{-2} . The frequency range for testing is from 100 kHz to 1 Hz.

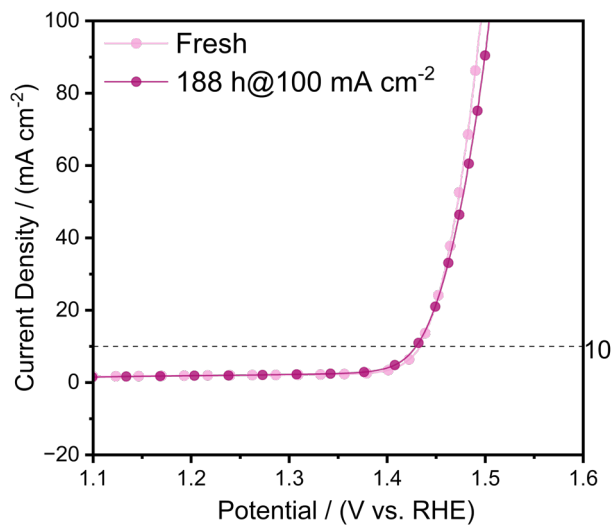


Figure S20 Polarization curves at the scan rate of 5 mV s^{-1} for $\text{Bi}_{0.05}\text{Ru}_{0.95}\text{O}_2$ electrode in 0.5 M H_2SO_4 electrolyte before and after 188-h stability test at 100mA cm^{-2} .

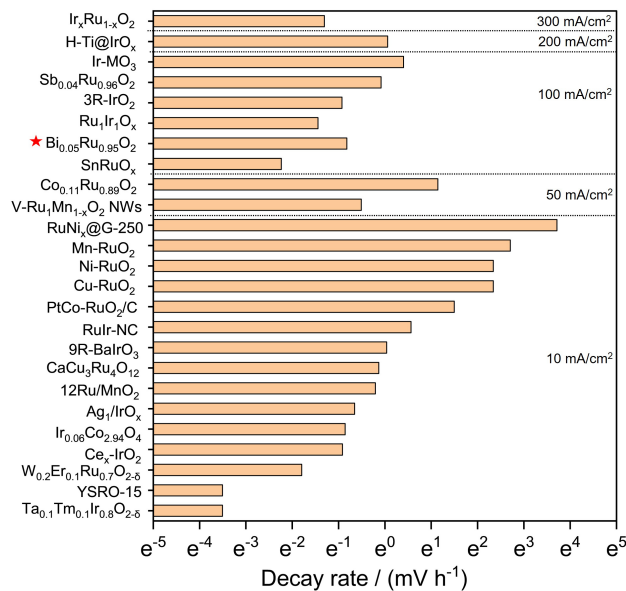


Figure S21 Comparison of decay rate (mV h⁻¹) between Bi_{0.05}Ru_{0.95}O₂, Sb_{0.04}Ru_{0.96}O₂ and recently-reported Ru- and Ir-based catalysts at their reported current density.

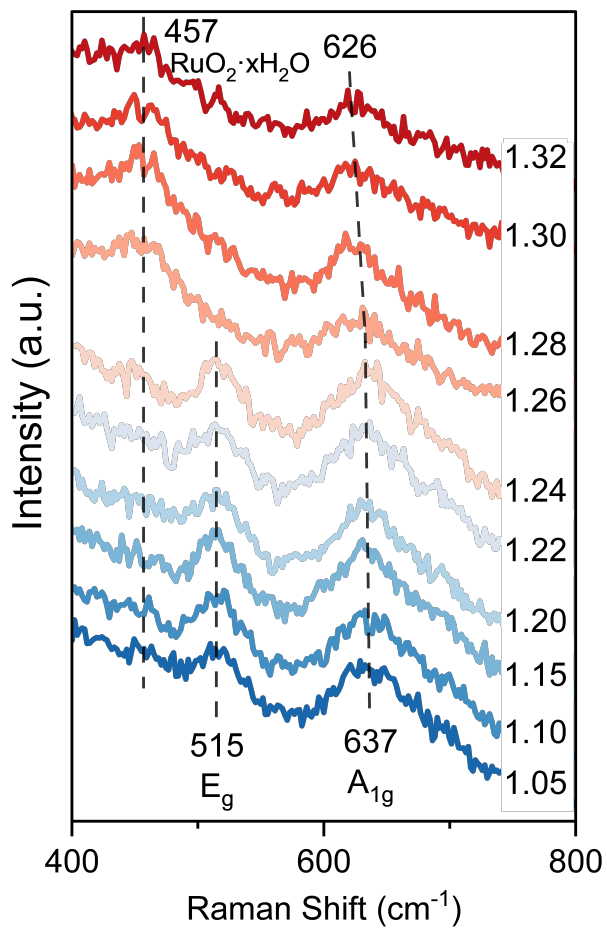


Figure S22. In-situ Raman spectra collected form $\text{Bi}_{0.05}\text{Ru}_{0.95}\text{O}_2$ catalyst in 0.1 M HClO_4 .

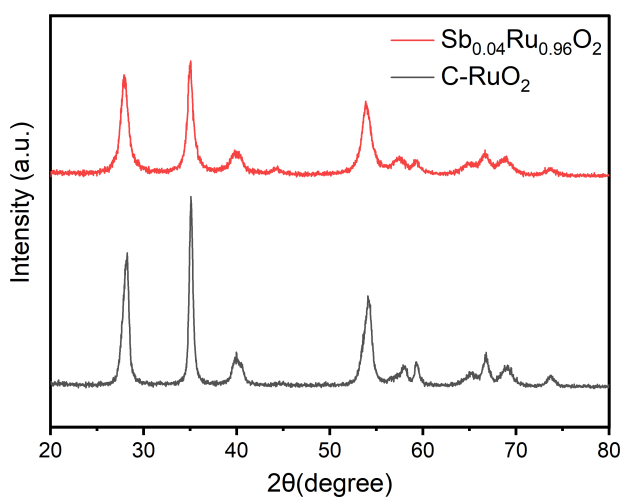


Figure S23 XRD patterns of $\text{Sb}_{0.04}\text{Ru}_{0.96}\text{O}_2$ and C-RuO₂.

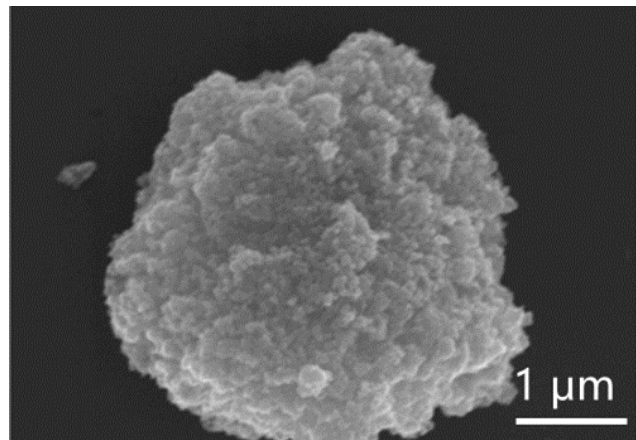


Figure S24 SEM image of $\text{Sb}_{0.04}\text{Ru}_{0.96}\text{O}_2$.

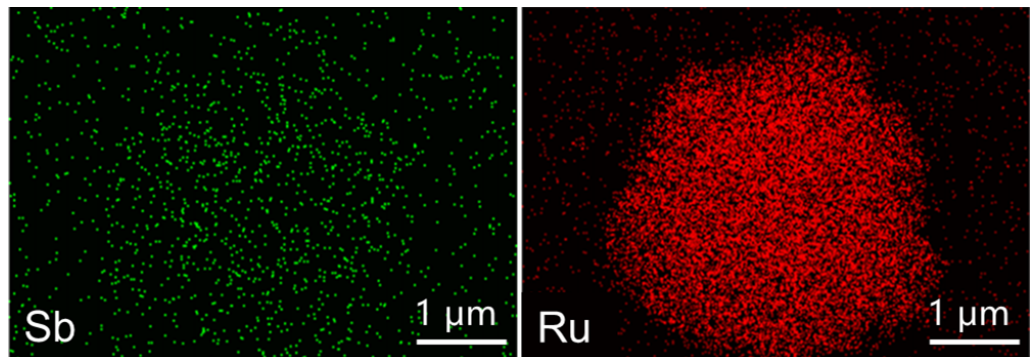


Figure S25 Element mapping of $\text{Sb}_{0.04}\text{Ru}_{0.96}\text{O}_2$.

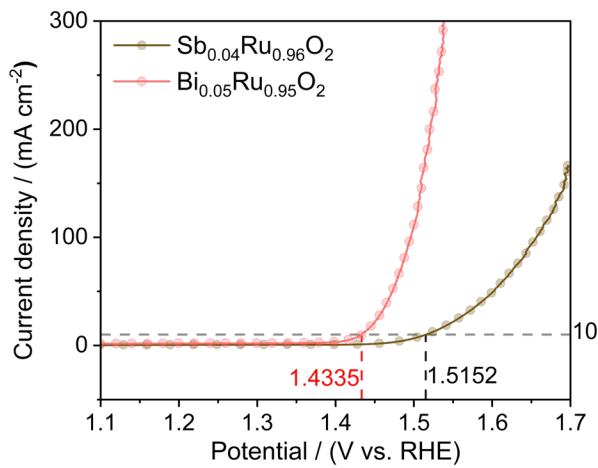


Figure S26 Polarization curves at the scan rate of 5 mV s⁻¹ for Sb_{0.04}Ru_{0.96}O₂ and Bi_{0.05}Ru_{0.95}O₂ electrodes in 0.5 M H₂SO₄ electrolyte.

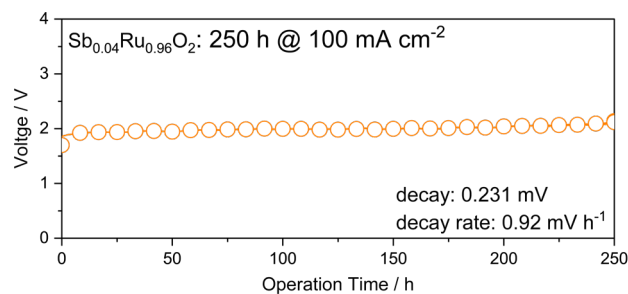


Figure S27 Stability test of Sb_{0.04}Ru_{0.96}O₂ electrode at the current density of 100 mA cm⁻² in 0.5 M H₂SO₄.

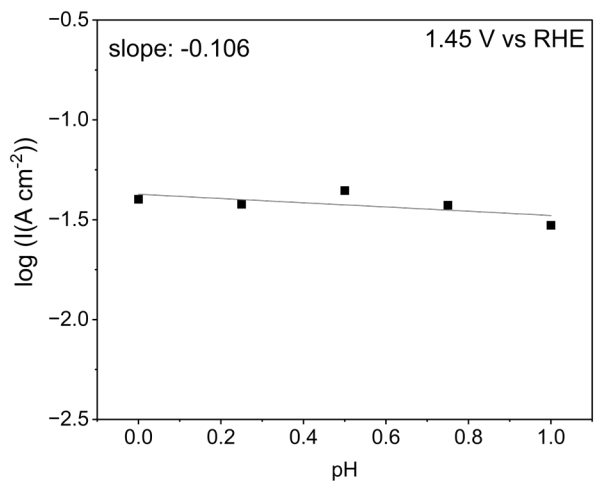


Figure S28 Log (I (A cm⁻²)) of $\text{Bi}_{0.05}\text{Ru}_{0.95}\text{O}_2$ electrode at 1.45 V vs. RHE as a function of pH.

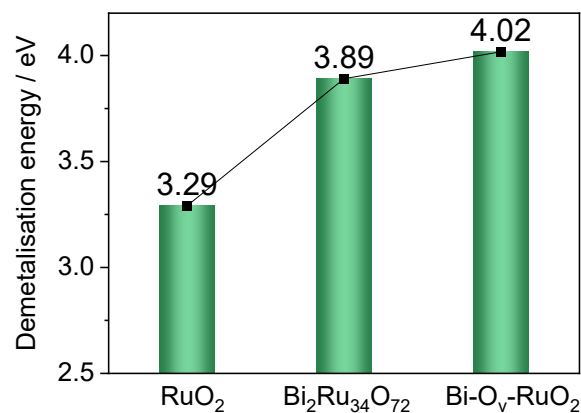


Figure S29 The demetalisation energies of RuO_2 , $\text{Bi}_2\text{Ru}_{34}\text{O}_{72}$ and $\text{Bi}-\text{O}_v-\text{RuO}_2$.

Table S1 The atomic ratio of Ru and Bi collected from EDS analysis of various $\text{Bi}_x\text{Ru}_{1-x}\text{O}_2$ samples.

Sample	Element	Atomic ratio [%]
$\text{Bi}_{0.03}\text{Ru}_{0.97}\text{O}_2$	Bi	2.50
	Ru	97.50
$\text{Bi}_{0.05}\text{Ru}_{0.95}\text{O}_2$	Bi	4.82
	Ru	95.18
$\text{Bi}_{0.10}\text{Ru}_{0.90}\text{O}_2$	Bi	9.90
	Ru	90.10

Table S2 Fitting results of the O 1s XPS spectra for $\text{Bi}_{0.05}\text{Ru}_{0.95}\text{O}_2$, HM-RuO₂ and C-RuO₂ (after carbon-correction).

Samples	O _L		M-OH		O _V		O _{ads}	
	Position /eV	Area (ratio)	Position /eV	Area (ratio)	Position /eV	Area (ratio)	Position /eV	Area (ratio)
C-RuO ₂	527.48	24156 (23.6%)	528.06	38244 (37.4%)	529.58	16210 (15.8%)	531.01	23742 (23.2%)
HM-RuO ₂	527.33	17551 (18.4%)	528.06	29686 (31.1%)	529.58	19745 (20.7%)	530.98	28473 (29.8%)
$\text{Bi}_{0.05}\text{Ru}_{0.95}\text{O}_2$	527.24	27824 (24.4%)	527.96	41922 (36.8%)	529.58	26244 (23.0%)	531.01	17996 (15.8%)

Table S3 Overpotential values collected from various $\text{Bi}_x\text{Ru}_{1-x}\text{O}_2$ electrode at 10 mA cm⁻².

Samples	Overpotential/mV
HM-RuO ₂	227.8
$\text{Bi}_{0.03}\text{Ru}_{0.97}\text{O}_2$	213.2
$\text{Bi}_{0.05}\text{Ru}_{0.95}\text{O}_2$	203.5
$\text{Bi}_{0.10}\text{Ru}_{0.90}\text{O}_2$	207.8
C-RuO ₂	403.0

Table S4 Comparison of C_{dl} values and the relative ratio to demonstrate the ECSA changes of various electrocatalysts.

Catalysts	$C_{dl} / [\text{mF cm}^{-2}]$	C_{dl} / C_s
$\text{Bi}_{0.03}\text{Ru}_{0.97}\text{O}_2$	62.98	1.05
$\text{Bi}_{0.05}\text{Ru}_{0.95}\text{O}_2$	163.94	2.73
$\text{Bi}_{0.10}\text{Ru}_{0.90}\text{O}_2$	222.71	3.71
$\text{Sb}_{0.04}\text{Ru}_{0.96}\text{O}_2$	186.74	3.11
C-RuO ₂	5.33	0.09
HM-RuO ₂	132.60	2.21

Table S5 The comparison of Tafel slope, overpotential and durability test performance of $\text{Bi}_{0.05}\text{Ru}_{0.95}\text{O}_2$ and HM-RuO₂ with recently reported electrocatalysts in 0.5 M H₂SO₄.

Catalyst	Tafel slope / (mV dec ⁻¹)	Overpotential / (mV)	Reference
Bi_{0.05}Ru_{0.95}O₂	52.90	203.5	This work
HM-RuO₂	71.64	227.8	This work
Ru _{0.6} Cr _{0.2} Ti _{0.2} O ₂	58	267	<i>J Am Chem Soc</i> , 2024, 146 , 15740-15750 ⁴
Ru ₁ Ir ₁ O _x	71.3	204	<i>Advanced Energy Materials</i> , 2021, 11 , 2102883 ⁵
Ru-UiO-bpydc	78.3	200	<i>Chem</i> , 2023, 9 , 1882-1896 ⁶
(Ru, Mn) ₂ O ₃	68.7	168	<i>Nano Energy</i> , 2023, 115 , 108727 ⁷
SA Zn-RuO ₂	56	210	<i>Journal of Energy Chemistry</i> , 2024, 88 , 94-102 ⁸
Ru ₂ (S ₃ Se)	72	186	<i>Energy & Environmental Science</i> , 2024, 17 , 1885-1893 ⁹
CoO _x /RuO _x -CC	61.2	180	<i>Small</i> , 2023, 19 , e2302238 ¹⁰
9R-BaIrO ₃	80	230	<i>J Am Chem Soc</i> , 2021, 143 , 18001-18009 ¹¹

Table S6 The comparison of durability test performance of $\text{Bi}_{0.05}\text{Ru}_{0.95}\text{O}_2$ and $\text{Sb}_{0.04}\text{Ru}_{0.96}\text{O}_2$ with recently reported electrocatalysts in 0.5 M H_2SO_4 .

catalyst	current density / (mA cm ⁻²)	operation time / h	decay rate / (mV h ⁻¹)	reference
$\text{Bi}_{0.05}\text{Ru}_{0.95}\text{O}_2$	100	>300	0.44	This work
$\text{Sb}_{0.04}\text{Ru}_{0.96}\text{O}_2$	100	250	0.92	This work
$\text{Ru}_{0.6}\text{Cr}_{0.2}\text{Ti}_{0.2}\text{O}_2$	100	200	0.025	<i>J Am Chem Soc</i> , 2024, 146 , 15740-15750 ⁴
$\text{Ru}_1\text{Ir}_1\text{O}_x$	100	110	0.236	<i>Advanced Energy Materials</i> , 2021, 11 , 2102883 ⁵
Ru-U _i O-bpydc	50	140	0.894	<i>Chem</i> , 2023, 9 , 1882-1896 ⁶
$(\text{Ru}, \text{Mn})_2\text{O}_3$	10	40	5.06	<i>Nano Energy</i> , 2023, 115 , 108727 ⁷
SA Zn-RuO ₂	10	43	4.32	<i>Journal of Energy Chemistry</i> , 2024, 88 , 94-102 ⁸
$\text{Ru}_2(\text{S}_3\text{Se})$	10	50	Stable	<i>Energy & Environmental Science</i> , 2024, 17 , 1885-1893 ⁹
CoO _x /RuO _x -CC	10	60	0.786	<i>Small</i> , 2023, 19 , e2302238 ¹⁰
9R-BaIrO ₃	10	48	1.04	<i>J Am Chem Soc</i> , 2021, 143 , 18001-18009 ¹¹
SnRuO _x	100	250	0.107	<i>Nat Commun</i> , 2023, 14 , 843 ¹²
3R-IrO ₂	100	42	0.396	<i>Joule</i> , 2021, 5 , 3221-3234 ¹³
Ir-MoO ₃	100	48	1.496	<i>Nat Commun</i> , 2021, 12 , 5676 ¹⁴
V-Ru _x Mn _{1-x} O ₂ NWs	50	101	0.6	<i>Journal of Materials Chemistry A</i> , 2023, 11 , 25252-25261 ¹⁵
Sm ₃ IrO ₇	10	10	24.02	<i>ACS Applied Materials & Interfaces</i> , 2023, 15 , 14282-14290 ¹⁶
MD-RuO ₂ -BN	10	24	1.2	<i>Nat Commun</i> , 2024, 15 , 3928 ¹⁷
RuIr-NC	10	40	1.759	<i>Nat Commun</i> , 2021, 12 , 1145 ¹⁸

$\text{Nd}_{0.1}\text{RuO}_x/\text{CC}$	10	25	0.6	<i>Advanced Functional Materials</i> , 2023, 33 , DOI: 10.1002/adfm.202213304 ¹⁹
Y_2MnRuO_7	10	40	0.3	<i>Nat Commun</i> , 2023, 14 , 2010 ²⁰
$\text{Li}_{0.52}\text{RuO}_2$	10	70	1.694	<i>Nat Commun</i> , 2022, 13 , 3784 ²¹
RuCoO_x	10	100	0.45	<i>J Am Chem Soc</i> , 2023, 145 , 17995-18006 ²²
Mn-RuO ₂ -450	10	150	0.267	<i>Small</i> , 2024, 20 , e2400754 ²³
$\text{RuO}_{2-x}/\text{RuSe}_2$	10	200	Stable	<i>Advanced Functional Materials</i> , 2024, DOI: 10.1002/adfm.202406587 ²⁴
12Ru/MnO ₂	10	200	0.815	<i>Nature Catalysis</i> , 2021, 4 , 1012-1023 ²⁵
PtCo-RuO ₂ /C	10	20	4.47	<i>Energy & Environmental Science</i> , 2022, 15 , 1119-1130 ²⁶
Ag_1/IrO_x	10	50	0.52	<i>ACS Energy Letters</i> , 2021, DOI: 10.1021/acsenergylett.1c00283, 1588-1595 ²⁷
Ni-RuO ₂	10	8	10.4	<i>Nat Mater</i> , 2023, 22 , 100-108 ²⁸
$\text{Ir}_{0.06}\text{Co}_{2.94}\text{O}_4$	10	200	0.424	<i>J Am Chem Soc</i> , 2021, 143 , 5201-5211 ²⁹

Table S7 The atomic ratio of Ru and Sb collected from EDS analysis of $\text{Sb}_{0.04}\text{Ru}_{0.96}\text{O}_2$ sample.

Sample	Element	Atomic ratio [%]
$\text{Sb}_{0.04}\text{Ru}_{0.96}\text{O}_2$	Sb	4.14
	Ru	95.86

Table S8 Relative Gibbs free energy of intermediates for AEM and LOM of $\text{Bi}_2\text{Ru}_{34}\text{O}_{72}$, $\text{Bi}-\text{O}_v-\text{RuO}_2$ and RuO_2 .

AEM			
Intermediates \ Model	RuO_2	$\text{Bi}_2\text{Ru}_{34}\text{O}_{72}$	$\text{Bi}-\text{O}_v-\text{RuO}_2$
Slab	0	0	0
*OH	1.35	0.88	0.66
*O	2.21	2.42	2.21
*OOH	4.23	4.05	3.63
Slab+O ₂	4.92	4.92	4.92

LOM			
Intermediates \ Model	RuO_2	$\text{Bi}_2\text{Ru}_{34}\text{O}_{72}$	$\text{Bi}-\text{O}_v-\text{RuO}_2$
Slab	0	0	0
*OH	1.35	0.88	0.66
*O	2.21	2.42	2.21
*H	5.66	5.28	4.69
Slab+O ₂	4.92	4.92	4.92

References

1. J. Rossmeisl, A. Logadottir and J. K. Nørskov, *Chemical Physics*, 2005, **319**, 178-184.
2. I. C. Man, H. Y. Su, F. Calle - Vallejo, H. A. Hansen, J. I. Martínez, N. G. Inoglu, J. Kitchin, T. F. Jaramillo, J. K. Nørskov and J. Rossmeisl, *ChemCatChem*, 2011, **3**, 1159-1165.
3. S. Liu, Y. Chang, N. He, S. Zhu, L. Wang and X. Liu, *ACS Appl Mater Interfaces*, 2023, **15**, 20563-20570.
4. J. Abed, J. Heras-Domingo, R. Y. Sanspeur, M. Luo, W. Alnoush, D. M. Meira, H. Wang, J. Wang, J. Zhou, D. Zhou, K. Fatih, J. R. Kitchin, D. Higgins, Z. W. Ulissi and E. H. Sargent, *J Am Chem Soc*, 2024, **146**, 15740-15750.
5. J. He, X. Zhou, P. Xu and J. Sun, *Advanced Energy Materials*, 2021, **11**, 2102883.
6. N. Yao, H. Jia, J. Zhu, Z. Shi, H. Cong, J. Ge and W. Luo, *Chem*, 2023, **9**, 1882-1896.
7. Y. Qin, B. Cao, X.-Y. Zhou, Z. Xiao, H. Zhou, Z. Zhao, Y. Weng, J. Lv, Y. Liu, Y.-B. He, F. Kang, K. Li and T.-Y. Zhang, *Nano Energy*, 2023, **115**, 108727.
8. Q. Qin, T. Wang, Z. Li, G. Zhang, H. Jang, L. Hou, Y. Wang, M. Gyu Kim, S. Liu and X. Liu, *Journal of Energy Chemistry*, 2024, **88**, 94-102.
9. D. Chen, H. Zhao, R. Yu, K. Yu, J. Zhu, J. Jiao, X. Mu, J. Yu, J. Wu and S. Mu, *Energy & Environmental Science*, 2024, **17**, 1885-1893.
10. L. Deng, S. Liu, D. Liu, Y. M. Chang, L. Li, C. Li, Y. Sun, F. Hu, H. Y. Chen, H. Pan and S. Peng, *Small*, 2023, **19**, e2302238.
11. N. Li, L. Cai, C. Wang, Y. Lin, J. Huang, H. Sheng, H. Pan, W. Zhang, Q. Ji, H. Duan, W. Hu, W. Zhang, F. Hu, H. Tan, Z. Sun, B. Song, S. Jin and W. Yan, *J Am Chem Soc*, 2021, **143**, 18001-18009.
12. Z. Shi, J. Li, Y. Wang, S. Liu, J. Zhu, J. Yang, X. Wang, J. Ni, Z. Jiang, L. Zhang, Y. Wang, C. Liu, W. Xing and J. Ge, *Nat Commun*, 2023, **14**, 843.
13. Z. Fan, Y. Ji, Q. Shao, S. Geng, W. Zhu, Y. Liu, F. Liao, Z. Hu, Y.-C. Chang, C.-W. Pao, Y. Li, Z. Kang and M. Shao, *Joule*, 2021, **5**, 3221-3234.
14. X. Liu, S. Xi, H. Kim, A. Kumar, J. Lee, J. Wang, N. Q. Tran, T. Yang, X. Shao, M. Liang, M. G. Kim and H. Lee, *Nat Commun*, 2021, **12**, 5676.
15. H. Zhu, Y. Wang, Z. Jiang, B. Deng and Z.-J. Jiang, *Journal of Materials Chemistry A*, 2023, **11**, 25252-25261.
16. Y. Wang, Z. Li, L. Hou, Y. Wang, L. Zhang, T. Wang, H. Liu, S. Liu, Q. Qin and X. Liu, *ACS Applied Materials & Interfaces*, 2023, **15**, 14282-14290.

17. D. Chen, R. Yu, K. Yu, R. Lu, H. Zhao, J. Jiao, Y. Yao, J. Zhu, J. Wu and S. Mu, *Nat Commun*, 2024, **15**, 3928.
18. D. Wu, K. Kusada, S. Yoshioka, T. Yamamoto, T. Toriyama, S. Matsumura, Y. Chen, O. Seo, J. Kim, C. Song, S. Hiroi, O. Sakata, T. Ina, S. Kawaguchi, Y. Kubota, H. Kobayashi and H. Kitagawa, *Nat Commun*, 2021, **12**, 1145.
19. L. Li, G. Zhang, J. Xu, H. He, B. Wang, Z. Yang and S. Yang, *Advanced Functional Materials*, 2023, **33**.
20. D. Galyamin, J. Torrero, I. Rodriguez, M. J. Kolb, P. Ferrer, L. Pascual, M. A. Salam, D. Gianolio, V. Celorio, M. Mokhtar, D. Garcia Sanchez, A. S. Gago, K. A. Friedrich, M. A. Pena, J. A. Alonso, F. Calle-Vallejo, M. Retuerto and S. Rojas, *Nat Commun*, 2023, **14**, 2010.
21. Y. Qin, T. Yu, S. Deng, X. Y. Zhou, D. Lin, Q. Zhang, Z. Jin, D. Zhang, Y. B. He, H. J. Qiu, L. He, F. Kang, K. Li and T. Y. Zhang, *Nat Commun*, 2022, **13**, 3784.
22. W. Zhu, F. Yao, K. Cheng, M. Zhao, C. J. Yang, C. L. Dong, Q. Hong, Q. Jiang, Z. Wang and H. Liang, *J Am Chem Soc*, 2023, **145**, 17995-18006.
23. M. Xiao, J. Liu, R. Li, Y. Sun, F. Liu, J. Gan and S. Gao, *Small*, 2024, **20**, e2400754.
24. Y. Chen, Y. Liu, L. Li, T. Sakthive, Z. Guo and Z. Dai, *Advanced Functional Materials*, 2024, DOI: 10.1002/adfm.202406587.
25. C. Lin, J.-L. Li, X. Li, S. Yang, W. Luo, Y. Zhang, S.-H. Kim, D.-H. Kim, S. S. Shinde, Y.-F. Li, Z.-P. Liu, Z. Jiang and J.-H. Lee, *Nature Catalysis*, 2021, **4**, 1012-1023.
26. H. Jin, S. Choi, G. J. Bang, T. Kwon, H. S. Kim, S. J. Lee, Y. Hong, D. W. Lee, H. S. Park, H. Baik, Y. Jung, S. J. Yoo and K. Lee, *Energy & Environmental Science*, 2022, **15**, 1119-1130.
27. F.-F. Zhang, C.-Q. Cheng, J.-Q. Wang, L. Shang, Y. Feng, Y. Zhang, J. Mao, Q.-J. Guo, Y.-M. Xie, C.-K. Dong, Y.-H. Cheng, H. Liu and X.-W. Du, *ACS Energy Letters*, 2021, DOI: 10.1021/acsenergylett.1c00283, 1588-1595.
28. Z. Y. Wu, F. Y. Chen, B. Li, S. W. Yu, Y. Z. Finfrock, D. M. Meira, Q. Q. Yan, P. Zhu, M. X. Chen, T. W. Song, Z. Yin, H. W. Liang, S. Zhang, G. Wang and H. Wang, *Nat Mater*, 2023, **22**, 100-108.
29. J. Shan, C. Ye, S. Chen, T. Sun, Y. Jiao, L. Liu, C. Zhu, L. Song, Y. Han, M. Jaroniec, Y. Zhu, Y. Zheng and S. Z. Qiao, *J Am Chem Soc*, 2021, **143**, 5201-5211.